

Examination of ionic wind and cathode sheath effects in a E-field premixed flame with ion density measurements

Stewart V. Jacobs and Kunning G. Xu

Citation: *Physics of Plasmas* **23**, 043504 (2016); doi: 10.1063/1.4945614

View online: <http://dx.doi.org/10.1063/1.4945614>

View Table of Contents: <http://scitation.aip.org/content/aip/journal/pop/23/4?ver=pdfcov>

Published by the [AIP Publishing](#)

Articles you may be interested in

[Stabilization of a lean premixed flame using non-thermal plasma](#)

J. Appl. Phys. **115**, 223304 (2014); 10.1063/1.4872471

[Characterization of an RF plasma ion source for ion implantation](#)

AIP Conf. Proc. **1496**, 316 (2012); 10.1063/1.4766552

[Measurement of electron temperature and ion density using the self-bias effect in plasmas](#)

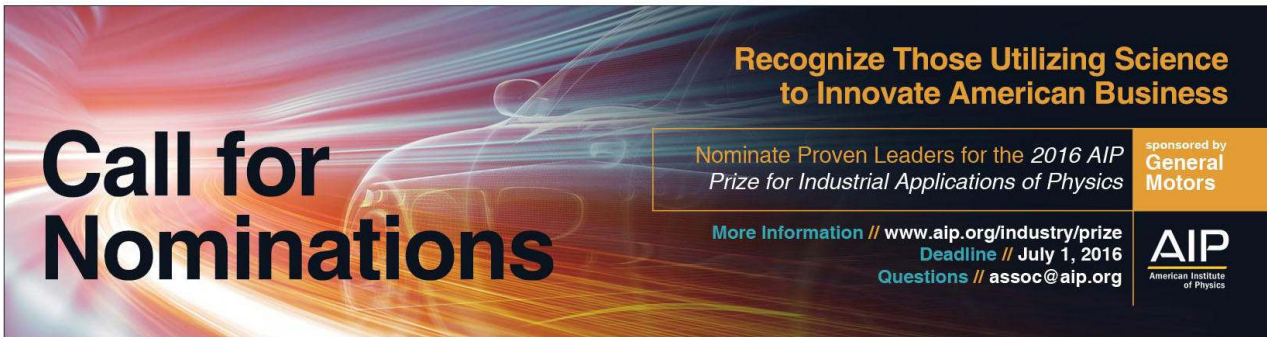
Phys. Plasmas **17**, 063501 (2010); 10.1063/1.3430632

[Effects of fast monoenergetic electrons on the ion dynamics near the cathode in a pulsed direct current plasma sheath](#)

Phys. Plasmas **15**, 033503 (2008); 10.1063/1.2895380

[Monitoring sheath voltages and ion energies in high-density plasmas using noninvasive radio-frequency current and voltage measurements](#)

J. Appl. Phys. **95**, 4593 (2004); 10.1063/1.1687975



Call for Nominations

Recognize Those Utilizing Science to Innovate American Business

Nominate Proven Leaders for the 2016 AIP Prize for Industrial Applications of Physics

More Information // www.aip.org/industry/prize
Deadline // July 1, 2016
Questions // assoc@aip.org

sponsored by General Motors

AIP
American Institute of Physics

Examination of ionic wind and cathode sheath effects in a E-field premixed flame with ion density measurements

Stewart V. Jacobs^{a)} and Kunning G. Xu^{b)}

University of Alabama in Huntsville, Huntsville, Alabama 35899, USA

(Received 25 August 2015; accepted 18 March 2016; published online 8 April 2016)

The effect of the ionic wind on a premixed methane-air flame under a DC electric field is studied via mapping of the ion density with Langmuir probes. Ion densities were observed to increase near the burner with increasing electrode voltage up to 6 kV. Past this electrode supply voltage, ion densities ceased increasing and began to decline in some locations within the premixed flame. The increased ion density is caused by an increase in ionic wind force and cathode sheath thickness. The plateau in density is due to the cathode sheath fully encompassing the flame front which is the ion source, thereby collecting all ions in the flame. The spatial density data support the ionic wind hypothesis and provide further explanation of its limits based on the plasma sheath. © 2016 AIP Publishing LLC. [<http://dx.doi.org/10.1063/1.4945614>]

I. INTRODUCTION AND BACKGROUND

Hydrocarbon flame sensitivity to electric fields has been the subject of extensive study for several decades. Research published by Wilson¹ demonstrated that hydrocarbon flames have electrical properties which can be manipulated through external fields. Later investigation led to the formulation of the ionic wind hypothesis to explain the observed changes in the flame. Lawton and Weinberg² expounded this hypothesis and provided calculations of the maximum pressures exerted by the ionic wind upon the flame. Current research efforts into this phenomenon, known as plasma-assisted combustion (PAC), have demonstrated significant promise for the development of more efficient combustors. Ganguly³ demonstrated that an electric field can sustain combustion in an ultra-lean Bunsen burner flame when it would otherwise quench. Liu *et al.*⁴ also describe this occurring, along with an increased rich flammability limit for propane flames. Similar results were reported by Kim *et al.*,⁵ who reported significant increases in the flame's blowoff velocity, and Volkov *et al.*,⁶ who described the electric field's ability to counteract thermoacoustic instabilities. Other effects of interest include an observed reduction in soot and pollution⁷⁻⁹ as well as changes to the flame speed and temperature profile of the flame.^{3,10-12} Typically, these observations are conducted using a positively biased electrode, but significant changes to the flame speed have been observed with negatively biased electrodes as well.¹³ Furthermore, changes to properties, such as flame speed, were observed with an input electrical power of a few Watts.^{10,14-16}

Two primary hypotheses exist to explain how an electric field affects the combustion process. The first is the ionic wind hypothesis, which proposes that the changes in flame behavior are linked to a stream of ions pushed by the electric field. The changes in the flame are then brought about by ion-ion and ion-neutral collisions. The collisions transfer the

energy gained from the electric field from electrostatic acceleration into increased neutral particle momentum. Momentum exchange from electron collisions is typically ignored due to the mass difference between electrons and ions or neutrals. A majority of research into electric field modified flames credit the ionic wind as either the sole explanation or a significant contributor to the observed flame changes,^{5,6,9,17,18} even in flames without a hydrocarbon fuel.¹⁵ Recent research has proposed modifications to the ionic wind hypothesis to better account for the influence of anion collisions.⁵ A competing hypothesis states that the observed flame changes are chemistry-driven instead of momentum-driven. The maximum pressure exerted by the ionic wind as catalogued by Lawton and Weinberg² was 0.0004 atm. Marcum and Ganguly¹⁰ argue that this is an insufficient pressure to account for some of the more significant changes to the flame. Instead, the electric field's effects on the flame are ascribed to the ions being forced towards the flame's preheat zone. Ions then undergo dissociative recombination with electrons and produce combustion radicals such as OH.¹⁰ The new radicals can then react with the fresh fuel/oxidizer mix and initiate chain branching or propagation reaction that, for example, increase flame speed. This mechanism is supported by later work by Marcum, Ganguly, and Wisman^{3,10,14} as well as Boom *et al.*¹¹

In this paper, we address the effect of the ionic wind in a premixed flame based on the growth of the burner plasma sheath. Experimental measurements of the ion density profile are compared to theoretical calculations of the sheath thickness. The goal is to explain why ion densities change in response to an electric field and compare the results against the predictions of prior hypotheses.

II. EXPERIMENTAL SETUP

The experimental apparatus consists of a cylindrical burner with a gridded surface, a high voltage DC power supply, a source-meter, a DAQ system, a single filament Langmuir probe, and a linear two axis stage used to automatically traverse the Langmuir probe through the flame.

^{a)}svj0001@uah.edu

^{b)}gabe.xu@uah.edu

The Langmuir probe is biased to -5 V by a Keithley 2410 source meter before being maneuvered into the flame. Data collection is managed by an Agilent 34972 DAQ system. Ion current measurements are derived from measuring the voltage across a $10\text{ M}\Omega$ resistor and applying Ohm's law. A schematic of the experiment is shown in Figure 1.

The burner is based on the flat flame burner design of Hartung *et al.*¹⁹ but runs without the shielding gas. The burner made from a naval brass cylinder with an inner diameter of 4.75 cm and is 7.62 cm long to allow for the reactants to become well premixed. Steel wool is placed at the bottom of the chamber to promote reactant mixing. The burner surface is a sheet of perforated brass with 0.50 mm diameter holes with a 22% open area fraction. The burner grid curves slightly when exposed to the flame and so is not perfectly flat. A $1/4\text{ in.}$ copper tube is soldered around the burner lip and connected to a water pump to cool the burner.

The positively biased electrode positioned 7.62 cm above the burner surface was used to generate the DC electric field between the electrode and the burner. This electrode polarity was chosen because the majority of previous work with electric field modification of hydrocarbon flames uses a positively biased electrode downstream of the flame and because the opposite polarity has not consistently been shown to have significant effects on the flame. The burner is thus the cathode and is connected to the true earth ground along with the high voltage DC power supply (Matsusada AU-10P60 series). The electrode used for this purpose is a $7.78 \times 7.78\text{ cm}$ grid electrode made from perforated steel sheet. It is connected to the high voltage DC power supply, which provides a bias up to 10 kV and is current limited to 60 mA during the experiment. This configuration produces a range of reduced electric field values up to 38 Td .

Methane is used as the fuel and compressed air as the oxidizer. Methane is used due to the extensive body of research on methane flames, and because hydrogen flames do not produce a sufficiently large number of ions without doping. Control of the equivalence ratio, the ratio of oxidizer to fuel compared against the oxidizer to fuel ratio of a

stoichiometric flame, is achieved through the use of two MKS 2179 mass flow controllers. The mixture ratio was maintained at stoichiometric. The total flow rate entering the burner was 7.53 SLM .

The Langmuir probe used to obtain ion density measurements is constructed from a 0.13 mm diameter tungsten wire placed in a 1.6 mm outer diameter alumina tube and oriented perpendicular to the flame's center axis. The active length of wire protruding from the tube is 4.7 mm long. Additional copper wires are placed inside tube to hold the tungsten wire in place and provide electrical connection. The wire is then connected to the Keithley 2410 sourcemeter, which is used to apply a bias voltage to the probe. Measurements are taken from the edge of the burner to centerline, under the assumption of an axisymmetric flame. At each point, a minimum of 100 voltage readings are taken and averaged to produce a statistical average. After all measurements have been collected, the probe is removed from the flame to allow it to cool before moving to the next location. The removal of the probe from the flame to cool was necessary in order to reduce the error and to extend the life of the probe. A flame exposure time test indicated a probe exposure time of $<6\text{ s}$ prevented significant changes to the probe characteristics and allowed repeatable measurements. These steps are completed at progressively higher vertical positions until the maximum height of 5 mm above the burner is reached. A summary of the experiment's range of values is shown below in Table I.

III. RESULTS

A. Flame temperature measurements

Reactants are premixed before reacting, so the majority of combustion occurs within a narrow region just above the burner surface. This is the premixed flame. However, not all of the fuel will react before escaping the premixed flame. The remaining fuel mixes with ambient air downstream of the premixed flame and causes a secondary flame to form just above the premixed flame. This is the diffusion flame, and it is typically much larger than the premixed flame. This work is primarily concerned with the premixed flame which has a height of $\sim 5\text{ mm}$ above the burner surface.

Flame temperature was measured with a $1/16\text{ in.}$ diameter Inconel sheathed, ungrounded, type K thermocouple placed in the center of the premixed flame. The thermocouple sheath was connected to an external ground to prevent interference from the electric field. Thermocouples are subject to significant radiative heat losses, so it is necessary to apply corrections in order to obtain the actual temperature. One approach

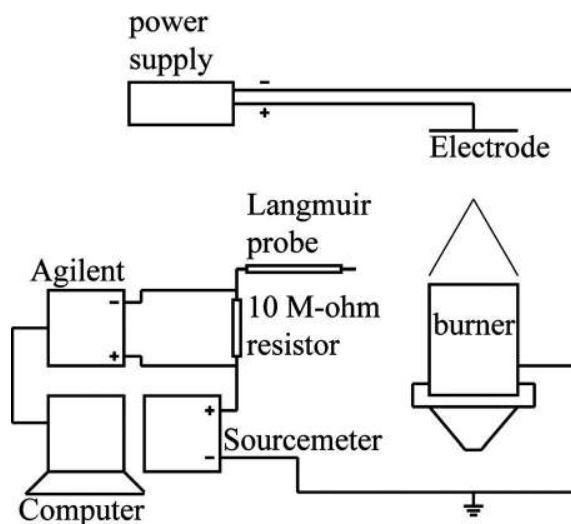


FIG. 1. Experimental setup.

TABLE I. Experimental test matrix.

Equivalence ratio	1.0
Supply voltages	0–10 kV
Radial probe positions	0–23.77 mm
Radial step size	0.91 mm
Axial probe positions	0–5 mm
Axial step size	1 mm

is to equate the convective transfer to the thermocouple to its radiative losses. This takes the form

$$h(T_f - T_{TC}) = \varepsilon\sigma(T_{TC}^4 - T_\infty^4), \quad (1)$$

where h is the convection coefficient, T_f is the flame temperature, T_{TC} is the thermocouple temperature, T_∞ is the free-stream air temperature, ε is the emissivity coefficient of the thermocouple, and σ is the Stefan-Boltzmann constant.

The thermocouple reads 1123 K at steady state for stoichiometric combustion. Using the properties of air and following the approach taken by Brundage *et al.*,²⁰ Eq. (1) yields a corrected temperature of 2153 K in the unmodified flame with no electric field. The burner's thermal power can be obtained from the volumetric flow rate and the heating value of methane which is taken as 37 710 kJ/m³. Using a flow rate of 7.53 SLM, the burner thermal power is 4.75 kW as designed.

B. Langmuir probe analysis

Methane flames have over 300 elementary reactions, many of which produce ions. A list of methane elementary reactions which produce ions in lean and stoichiometric flames and plots of the ion concentrations can be found in Prager *et al.*²¹ and Goodings *et al.*²² The dominant ion according to both is H_3O^+ , followed by CHO^+ and $\text{C}_2\text{H}_3\text{O}^+$. However, the concentration of H_3O^+ is almost a full order of magnitude larger than either of the other two species. Thus for simplicity H_3O^+ can be treated as the representative ion for the purposes of determining ion properties.

Using this assumption, it is possible to obtain ion concentrations from the ion current. For cylindrical probes with thick probe sheaths, Clements *et al.*²³ provide the following equation for the ion density

$$n_i = \left(\frac{I}{5.3(\epsilon_0\mu_i)^{0.25}V_b^{0.5}r_p^{0.25}l_p} \right)^{\frac{1}{0.75}} * \frac{1}{eU}, \quad (2)$$

where n_i is the ion density, I is the current, ϵ_0 is the permittivity of free space, μ_i is the ion mobility, V_b is the probe bias, r_p is the probe radius, l_p is probe length, e is the elementary charge, and U is the flow velocity. The ion mobility is assumed to have the mobility of H_3O^+ , which is $8.4 \times 10^{-4} \text{ m}^2/\text{V s}$.²⁴ The flow velocity is calculated to be 0.369 m/s, which is typical of methane flames at the equivalence ratios measured in the present work.

The Langmuir probe must be operating in the sheath-convection regime in order for Eq. (2) to be valid. In this regime, the conditions $Re_e\alpha_p^2\chi^2 \gg 1$ and $Re_e\alpha_p^2 < 1$ must be satisfied. If the sheath is to be treated as thick, the condition $\alpha_p\chi \gg 1$ must also be satisfied. A detailed discussion of this is provided by Smy,²⁵ who defines these quantities as follows:

$$Re_e = \frac{2r_p U e}{\mu_i k T_e}, \quad (3)$$

$$\alpha_p = \frac{\lambda_D}{r_p}, \quad (4)$$

$$\chi = \frac{eV_b}{kT_e}, \quad (5)$$

where Re_e is the electric Reynolds number, λ_D is the Debye length of the form $\sqrt{\epsilon_0 k T_e / n_e e^2}$, α_p is the ratio of the Debye length to the probe radius, χ is the dimensionless potential, k is the Boltzmann constant, T_e is electron temperature, and n_e is the bulk ionization density.

For this analysis, the electron temperature is assumed equal to the flame temperature and the ion mobility is assumed constant for the range of electric fields presented. A bias of -5 V was chosen for this analysis in order to ensure that the Langmuir probe was operating in the regime of complete ion saturation while not be so large as to start collecting significant numbers of ions far from the probe surface. As shown in Table II, these conditions also satisfy the conditions required to be operating in the sheath-convection regime. Under these conditions, the product $\alpha_p\chi$ is greater than 1, so the sheath must be treated as thick.

C. Ion density measurements

A distinct pattern emerges for ion densities in the premixed flame, as shown in Figure 2. Ion density is very low near the edge of the burner but generally increases closer to the flame's center axis. Applying the electric field greatly increases the ion density within the premixed flame, peaking at a supply voltage of 6 kV, and then declining as the field strength increases. The same pattern is repeated in Figure 3, which tracked ion densities 5 mm from the burner. Ion densities do increase, but the peak occurs at a supply voltage of 4 kV instead.

The set of gradient maps in Figure 4 show the ion density profile of the premixed flame. The solid black line is the approximate location of the premixed flame. The flame, in general, shows high concentration of ions along the surface of the burner grid near the flame's center axis, as well as between 5 mm and 10 mm from the burner edge. Increasing the electric field strength causes an order of magnitude gain in the ion density in both locations. Whereas the unmodified flame has a maximum ion density of $2 \times 10^{16} \text{ m}^{-3}$, this increases to $1 \times 10^{17} \text{ m}^{-3}$ under a supply voltage of 6 kV. This is accompanied by a significant loss of ion density outside of the premixed flame, particularly at supply voltages above 6 kV. This suggests downstream ions are being moved to the burner.

D. Error analysis

Uncertainties in the physical aspects of the system were either determined by measurements or by manufacturer specifications. The tungsten filament had an uncertainty in a diameter of $\pm 0.0019 \text{ mm}$, while the probe length had an uncertainty of 0.025 mm. Uncertainty in the Velmex position was determined by the minimum step size of each axis. The horizontal minimum step size was 0.025 mm, while the vertical minimum step size was 0.0064 mm.

TABLE II. Electric characteristics of the probe.

$Re_e\alpha_p^2\chi^2$	24.047
$Re_e\alpha_p^2$	0.033
$\alpha_p\chi$	8.737

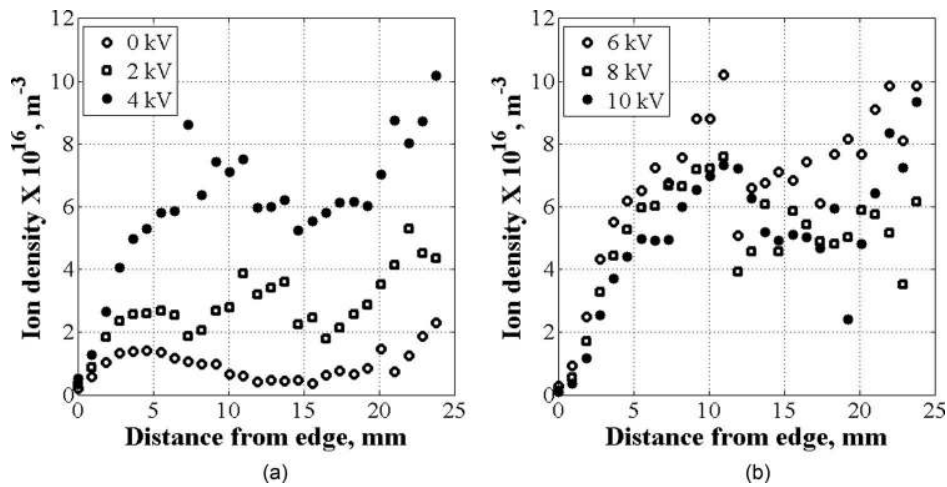


FIG. 2. Ion densities near the burner. The maximum ion density corresponds to an electrode supply voltage of 6 kV and 11 mm from the burner edge. (a) $V_{ss} = 0\text{--}4$ kV. (b) $V_{ss} = 6\text{--}10$ kV.

Uncertainties for the stoichiometric flame are shown in Table III. The uncertainties calculated here show both a spatial dependence and a voltage dependence similar to the mean ion densities in both locations. At 0 mm, uncertainties tend to be very similar, regardless of electrode supply voltage, although some variability is present. This is not the case at 5 mm, where the uncertainty of the probe sometimes exceeds 100%. This can be attributed to the probe registering positive currents during operation when it should be registering only negative currents. Close to the boundary of the premixed flame, therefore, the Langmuir probe may have accuracy problems in a strong electric field.

Probe integrity presents another possible source of error. Long term exposure to plasmas with high energy ions has been observed to cause sputtering damage to the surface of Langmuir probes, leading to portions of the probe becoming nonconductive,²⁶ thereby reducing the effective surface area and altering the current-voltage response. The limited time period of exposure to flame (<6 s per location), combined with the low energy of ions in the flame, should mean that sputtering damage is not a concern for this work.

While material deposition on the probe surface from the combustion products presents another possible source of error, as the measurements were taken primarily within the reactant region or just downstream of the premixed flame front, the presence of soot or other solid combustion products is minimal.

The most likely deposited material is carbon, which due to its conductive nature would increase the surface area of the probe. This can cause the ion density to be over-calculated. However, no obvious deposits were observed on the probe, only some discoloration of the tungsten due to the heat. At most, there could be a layer of carbon a few μm thick which would increase the effective surface area by only a few percent. This would not account for the magnitude of changes observed in the results. As the results show, the ion density increases then plateaus, as opposed to a continual increase if a significant layer of carbon was deposited during data collection.

It should be noted that a detailed chemical or microscope examination of the probe tip was not done and the nature of the discoloration is not fully known. The surface discoloration of the probe may be due to carbon deposition as noted, but the carbon state is not clear and can cause different behaviors. For example, graphitic carbon is highly conductive, while amorphous carbon is not. Thus, the unknown nature of the surface may contribute to the uncertainty in the measurements.

IV. DISCUSSION

A. Comparison with literature

MacLachy²⁴ provides a list of prior attempts at measuring ion density using physical instruments, the majority of

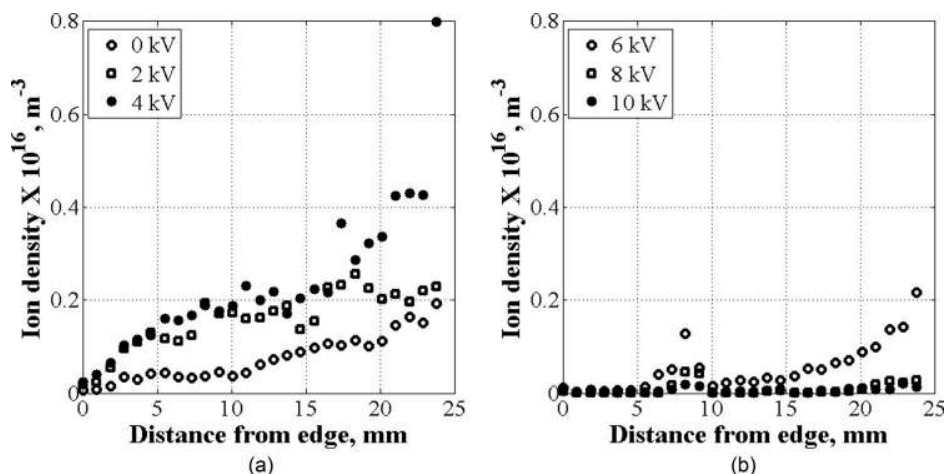


FIG. 3. Ion densities 5 mm above the burner. The maximum ion density corresponds to an electrode supply voltage of 4 kV and occurs near the center axis of the flame. (a) $V_{ss} = 0\text{--}4$ kV. (b) $V_{ss} = 6\text{--}10$ kV.

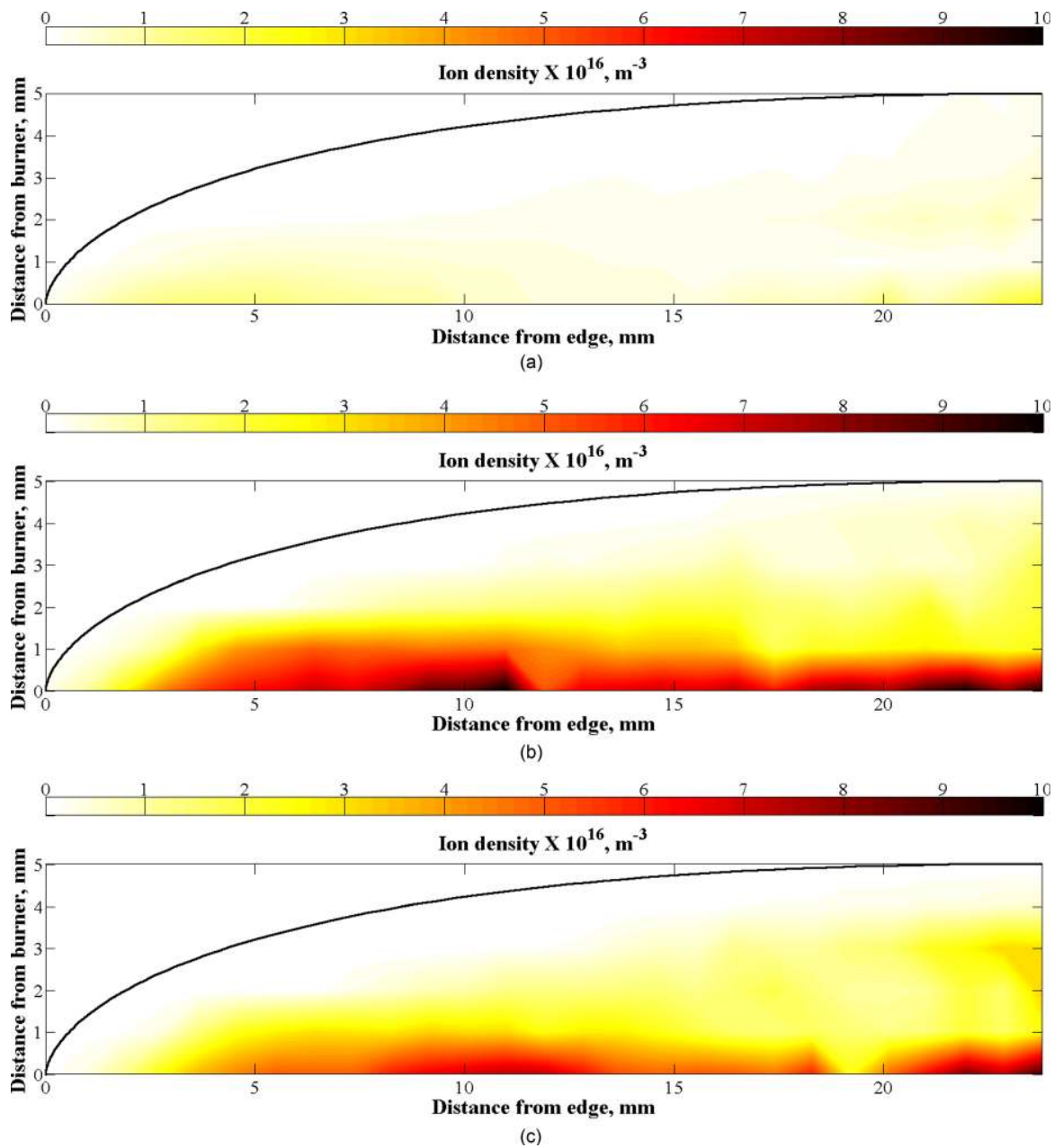


FIG. 4. Gradient map of ion densities. The solid black line represents the premixed flame. (a) $V_{ss} = 0$ kV. (b) $V_{ss} = 6$ kV. (c) $V_{ss} = 10$ kV.

them Langmuir probes. The closest match to our experiment comes from Wortberg²⁷ and Goodings *et al.*,²⁸ both of whom measured the ion density in a methane-air flame at atmospheric pressure. Wortberg measured a maximum density of $1.6 \times 10^{16} \text{ m}^{-3}$, and Goodings *et al.* measured $4 \times 10^{16} \text{ m}^{-3}$.

TABLE III. Uncertainties in Langmuir probe measurements.

	Uncertainty percentage of mean at 0 mm (m^{-3})	Uncertainty percentage of mean at 5 mm (m^{-3})
$V_{ss} = 0$ kV	17.9%	18.7%
$V_{ss} = 2$ kV	35.8%	39.9%
$V_{ss} = 4$ kV	24.4%	19.2%
$V_{ss} = 6$ kV	22.3%	67.7%
$V_{ss} = 8$ kV	20.3%	148%
$V_{ss} = 10$ kV	22.4%	251%

MacLachy uses a propane-air flame and records a maximum ion density of $4 \times 10^{17} \text{ m}^{-3}$, a full order of magnitude above both Goodings *et al.* and Wortberg. Direct numerical simulations of methane-air flames by Belhi *et al.*²⁹ and Prager *et al.*²¹ report very low peak ion densities of $1.3 \times 10^{16} \text{ m}^{-3}$. The plateau in change to the ion density, as seen in Figures 2 and 3 are similar to the work of Karnani and Dunn-Rankin,¹³ who observed the same effects at a similar electrode supply voltage using a non-premixed flame.

Data in the present work agree very well with the findings of previous authors. Discrepancies in ion density values are likely due to different experimental configurations. For example, previous investigators have used square Bunsen burners,²⁴ Perkin-Elmer burners,¹⁰ and nozzle-type burners,⁵ which can alter the distribution of particles. Additionally, ion densities from Belhi *et al.* and Prager

et al. trend lower due to the authors using a simulation with a very lean flame.

B. Assessment of mechanisms affecting ion behavior

1. Ionic wind effects

Ion densities near the burner begin increasing as soon as the electric field is applied, which is accompanied by decreases in the ion densities downstream of the flame. As prior authors have explained, this is the result of the ionic wind, which acts as a body force on the ions within the plasma. Ionic wind strength can be quantified by calculating its force density, represented as the quantity f . This equation, as described by Lawton and Weinberg,² takes the form

$$f = Ee n_i. \quad (6)$$

Here, the force density is a linear function of the electric field, thus a stronger electric field should produce a stronger ionic wind and lead to a higher ion density.

The ionic wind force density associated with the results of the present work is shown in Figure 5, which is calculated using the ion density and electric field measured at 0 mm. Ionic wind force density increases as more voltage is applied to the electrode as is expected. The force density shows rapid growth up to 6 kV. This is consistent with the expected results of Eq. (6), as well as the rapid surge in ion density near the burner. The ionic wind is therefore a significant factor in promoting ion density growth up to an electrode supply voltage of 6 kV. Dividing the force density by the electrode supply voltage yields the ionic wind efficiency. Here, the ionic wind efficiency ranges from $1.01 \text{ N m}^{-3} \text{ V}^{-1}$ to $2.15 \text{ N m}^{-3} \text{ V}^{-1}$, with an average value of $1.52 \text{ N m}^{-3} \text{ V}^{-1}$.

2. Cathode sheath effects

Since the ionic wind increases in strength with electric field, it would be anticipated that the ion densities would continuously increase. However, ion densities cease increasing after 6 kV has been applied to the electrode. In some

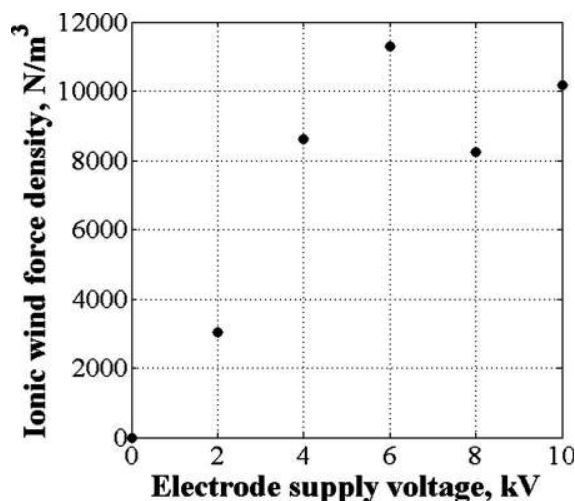


FIG. 5. Ionic wind strength expressed as a force density. The force density is calculated using the ion density and electric field near the burner surface.

locations within the flame, the ion densities continue to decrease past 6 kV. Neither should occur if the ionic wind is the only direct influence on ion densities. Additional influences upon the chemiionized plasma must therefore be considered.

One explanation for the ions not increasing is through the influence of the cathode sheath. The cathode plasma sheath is a boundary condition which exists between the bulk plasma and the cathode since the two are not held at the same potentials. Here, the bulk plasma is positive, around the biased voltage, and the cathode is a ground, so the cathode sheath has a very strong negative voltage gradient. Since the ionic wind is a function of electric field, this has the effect of making the ionic wind stronger in the cathode sheath than in the bulk plasma. The strong voltage gradients trap ions within the cathode sheath once they enter it. In conjunction with the ionic wind, the cathode sheath explains why the ion densities tend to concentrate so strongly, even though diffusion should prevent this from occurring.

The size of the cathode sheath in a flame plasmas is described by Xu,³⁰ and more generally for collisional plasmas by Sheridan and Goree.³¹ For a collisional plasma, the collision parameter α_c must be >1 , where α_c is defined as the ratio of the Debye length to the ion-neutral mean free path

$$\alpha_c = \frac{\lambda_D}{\lambda_{MFP}}, \quad (7)$$

and the ion-neutral mean free path is defined as the inverse product of the ion-neutral momentum transfer cross-section and the bulk ionization density

$$\lambda_{MFP} = \frac{1}{\sigma n}. \quad (8)$$

Momentum transfer cross-sections for H_3O^+ collisions are not available, so the $\text{N}_2\text{-N}_2^+$ cross-section will be used instead. Assuming an electron temperature equal to the flame temperature, the momentum transfer cross-section is $1.41 \times 10^{-18} \text{ m}^2$.³²

The approach taken by Xu describes the cathode sheath thickness for a collisional plasma as

$$D = \lambda_D \left[\frac{500 \chi_s^3}{243 \alpha_c u_0^2} \right]^{1/5}, \quad (9)$$

where the dimensionless potential of the sheath χ_s is based on the sheath potential drop, the non-dimensionalized ion speed at sheath entry u_0 is ~ 1 , and the collision parameter α_c is 154 for this plasma. For these conditions, the sheath thickness is plotted as a function of electrode supply voltage in Figure 6. Here, the cathode sheath thickness starts to encompass the 5 mm tall premixed flame after a 4 kV potential has been applied. After 6 kV has been applied, the cathode sheath encloses both the premixed flame and a small segment downstream of it. Ions densities fall off rapidly downstream of the premixed flame, with many ion species either completely disappearing or becoming significantly reduced.²²

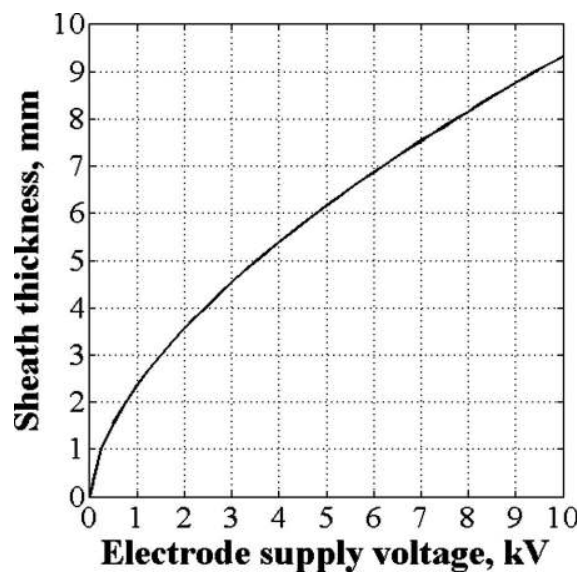


FIG. 6. Cathode sheath thickness growth as a function of electrode supply voltage assuming electrons are in thermal equilibrium with the flame. The sheath thickness outgrows the flame height by the time the electrode supply voltage reaches 4 kV.

3. Electron impact dissociation effects

Electron impact dissociation, wherein electron impacts with neutrals cause dissociation, is another possible contender for processes which influence flame behavior. The process has been observed in gases which would be abundant in hydrocarbon flames, including CH_4 ³³ and N_2 ,³⁴ and previous work^{3,11} has identified impact dissociation as a source of combustion radicals. In order for electron impact dissociation to take place, electrons must have sufficient energy. In many experiments, the minimum energy required for this to be nontrivial is 12 eV. Assuming electrons are produced with a temperature equivalent to that of the flame, insufficient energy would be available, since this leaves electrons with an energy in the order of 0.2 eV. The electric field inside the sheath would be sufficient for electrons to acquire the required energy to induce impact dissociation. However, the sheath is electron-repelling, and a majority of electrons are produced within the flame before being pushed downstream. Electron impact dissociation would potentially be a mechanism of interest, but its effects would largely be confined to regions downstream of the premixed flame and thus would not strongly influence the premixed flame, if at all.

4. Summary

Based upon these results, changes in ion density within a flat flame follow a distinct pattern controlled by the strength of a positive DC electric field and the growth of the cathode plasma sheath. At low voltages, the cathode sheath is thin and affects a small volume of the plasma. The electric field within the bulk plasma is small but sufficient to generate the ionic wind and push ions to the sheath. As ion production in a flame is through a chemical process which is largely independent of the electric field, there is a constant rate of ions entering the plasma. The ions will also diffuse

both upstream and downstream of the flame front, though the density will be higher downstream due to flow convection. The ionic wind thus depletes the downstream ions and moves them upstream towards the burner. With increased voltage, the cathode sheath grows, encompassing a larger volume and thus a larger portion of ions are subjected to the high electric field within the sheath, further pushing ions towards the burner. Eventually, the sheath grows thick enough to encompass the flame front where chemiionization and ion production occur. At this point, the ion source is inside the sheath and all ions that are produced are pushed to the burner. The sheath can grow a little more to collect the ions convected downstream by the flow. At this point, all ions are subject to the large sheath fields and further increases in voltage should not result in further increase in the ion density.

One final point to consider is the inverse ion gradient inside the sheath. In common low-pressure, uniform, volumetric plasmas, the ion density decreases closer to the surface or electrode. This occurs due to mass conservation requiring the flux, nv , in the sheath be constant. Thus inside the sheath as ions are acceleration and v increases, n must decrease. However, the densities measured here indicate the opposite, namely, the ion density is largest closer to the burner surface. This can be attributed to the two factors of a non-uniform plasma and high collisionality. Ion production in a flame is fixed at the flame front, which does not move here. The produced ions will diffuse both upstream and downstream of the flame front, though flow convection will greatly increase the ion density downstream. Thus as the cathode sheath grows toward the flame front, the ion density and thus flux at the sheath edge is not uniform and actually increases, assuming ions always enter the sheath at the Bohm velocity. This will result in a continual increase in the flux and thus density in the sheath. Second, the highly collisional nature of the flame plasma means the ion velocity is much lower than their low-pressure counterpart. The ion-neutral mean free path is in the order of $0.3 \mu\text{m}$, much smaller than the sheath thickness. As ions move upstream from the hot flame to the colder reactant flow, the lower temperature and slightly higher pressure will further increase the neutral density and thus collision rate. This all combines to significantly reduce the ion velocity in the sheath as they move closer to the burner. Thus just by conservation of mass, the density must increase to compensate, in addition to the ionic wind pushing more ions toward the burner.

The observed decrease in ion densities above 6 kV cannot be fully addressed at this time. The dissociative recombination hypothesis proposed by Marcum *et al.* offers a reasonable explanation for why ion density may decrease, since dissociative recombination consumes ions. However, that is not the focus of the present work.

V. CONCLUSION

A steady DC electric field was applied to a flat, methane-air flame under stoichiometric equivalence ratio. Ion densities were measured using a single wire Langmuir probe and high-pressure Langmuir probe theory. The data indicated that ion densities greatly increased with the

electrode supply voltage near the burner at the expense of ion densities downstream of the flame. This growth was attributed to the increasing ionic wind strength, which moved ions towards the burner and the growth of the burner plasma sheath. Ion density growth continued until the electrode supply voltage reached 6 kV, at which point ion densities ceased growing and started to decline in some locations. This was attributed to burner sheath encompassing the entire premixed flame and a significant proportion of the ion-containing space downstream of the premixed flame once the electrode supply voltage exceeded 6 kV. Comparatively few ions persist further downstream, thus ion density growth ceases due to fewer ions being trapped by the expanding cathode sheath. The results provide further support for the ionic wind effect as a dominant mechanism in electric field modified flames, and additionally, show the impact of the plasma sheath on the limit of the effect.

ACKNOWLEDGMENTS

This research was supported by the University of Alabama in Huntsville; the authors are very appreciative of this support. The authors would like to thank Roberto Dextre and Brian Roy for helping with data collection and processing and David Lineberry for providing support with the equipment.

¹H. Wilson, *Rev. Mod. Phys.* **3**, 156 (1931).

²J. Lawton and F. Weinberg, *Proc. R. Soc. A* **277**, 468 (1964).

³B. Ganguly, *Plasma Phys. Controlled Fusion* **49**, B239 (2007).

⁴L. Xingjian, H. Liming, Y. Jinlu, Z. Hao, and J. Tao, *J. Therm. Sci.* **24**, 283 (2015).

⁵K. Kim, S. Chung, and H. Kim, *Combust. Flame* **159**, 1151 (2012).

⁶E. Volkov, V. Kornilov, and L. de Goey, *Proc. Combust. Inst.* **34**, 955 (2013).

⁷M. Saito, M. Sato, and K. Sawada, *J. Electrostat.* **39**, 305 (1997).

⁸Y. Zhang, Y. Wu, H. Yang, H. Zhang, and M. Zhu, *Fuel* **109**, 350 (2013).

⁹A. Sakhrieh, G. Lins, F. Dinkelacker, T. Hammer, A. Leipertz, and D. Branston, *Combust. Flame* **143**, 313 (2005).

¹⁰S. Marcum and B. Ganguly, *Combust. Flame* **143**, 27 (2005).

¹¹J. Van den Boom, A. Konnov, A. Verhasselt, V. Kornilov, L. Degoeij, and H. Nijmeijer, *Proc. Combust. Inst.* **32**, 1237 (2009).

¹²M. Sánchez-Sanz, D. Murphy, and C. Fernandez-Pello, *Proc. Combust. Inst.* **35**, 3463 (2015).

¹³S. Karnani and D. Dunn-Rankin, *Combust. Flame* **162**, 2865 (2015).

¹⁴D. Wisman, S. Marcum, and B. Ganguly, *Combust. Flame* **151**, 639 (2007).

¹⁵Y. Gan, M. Wang, Y. Luo, X. Chen, and J. Xu, *Adv. Mech. Eng.* **8**, 1 (2016).

¹⁶H. Duan, X. Wu, T. Sun, B. Liu, J. Fang, C. Li, and Z. Gao, *Fuel* **158**, 807 (2015).

¹⁷F. Altendorfner, J. Kuhl, L. Zigan, and A. Leipertz, *Proc. Combust. Inst.* **33**, 3195 (2011).

¹⁸S. Ryu, Y. Kim, M. Kim, S. Won, and S. Chung, *Combust. Flame* **157**, 25 (2010).

¹⁹G. Hartung, J. Hult, and C. Kaminski, *Meas. Sci. Technol.* **17**, 2485 (2006).

²⁰A. Brundage, A. Donaldson, W. Gill, S. Kearney, V. Nicolette, and N. Yilmaz, *J. Fire Sci.* **29**, 195 (2011).

²¹J. Prager, U. Riedel, and J. Warnatz, *Proc. Combust. Inst.* **31**, 1129 (2007).

²²J. Goodings, D. Bohme, and N. Chun-Wai, *Combust. Flame* **36**, 27 (1979).

²³R. Clements, S. Rizvi, and P. Smy, *IEEE Trans. Plasma Sci.* **22**, 435 (1994).

²⁴C. MacLatchy, *Combust. Flame* **36**, 171 (1979).

²⁵P. Smy, *Adv. Phys.* **25**, 517 (1976).

²⁶E. Stamate and K. Ohe, *J. Vac. Sci. Technol., A* **20**, 661 (2002).

²⁷G. Wortberg, *Symp. (Int.) Combust., [Proc.]* **10**, 651 (1965).

²⁸J. Goodings, D. Bohme, and T. Sugden, *Symp. (Int.) Combust., [Proc.]* **16**, 891 (1977).

²⁹M. Belhi, P. Domingo, and P. Vervisch, *Combust. Flame* **157**, 2286 (2010).

³⁰K. Xu, *Combust. Flame* **161**, 1678 (2014).

³¹T. Sheridan and J. Goree, *Phys. Fluids B* **3**, 2796 (1991).

³²A. Phelps, *J. Phys. Chem. Ref. Data* **20**, 557 (1991).

³³M. Cha and Y. Lee, *IEEE Trans. Plasma Sci.* **40**, 3131 (2012).

³⁴Y. Itikawa, *J. Phys. Chem. Ref. Data* **35**, 31 (2006).